Journal of Alloys and Compounds 509 (2011) 7519–7524

Contents lists available at ScienceDirect

Journal of Alloys and Compounds

journal homepage: www.elsevier.com/locate/jallcom

Self-assembly of TiSi nanowires on $TiSi_2$ thin films by APCVD

Zhaodi Ren, Peng Hao, Jun Du, Gaorong Han, Wenjian Weng, Ning Ma, Piyi Du*

State Key Laboratory of Silicon Materials, Department of Materials Science and Engineering, Zhejiang University, Hangzhou 310027, China

ARTICLE INFO

Article history:
Received 3 December 2010
Received in revised form 19 April 2011
Accepted 20 April 2011
Available online 27 April 2011

Keywords:
Nanostructured materials
Titanium silicide
Vapor deposition
Crystal growth
Anisotropy

ABSTRACT

Titanium silicide thin films and nanowires (NWs) were prepared on a glass substrate using the APCVD method. Gaseous SiH_4 and $TiCl_4$ were used as precursors for Si and Ti, respectively. $TiSi_2$ thin films were precipitated on the glass substrate first, and then single-crystal TiSi NWs were grown on the $TiSi_2$ thin films as-prepared by controlling the concentrations of the source gases, SiH_4 and $TiCl_4$, without using any catalysts. The TiSi NWs were typically 1–2 μm long and 15–50 nm thick. The growth direction of the NWs was perpendicular to the (1 1 0) plane, in which a competition in growth rate among different crystallographic planes of the TiSi crystalline phase occurs. The oriented growth of the TiSi crystalline phases is responsible for the formation of the NWs.

© 2011 Elsevier B.V. All rights reserved.

1. Introduction

Metal silicides (MS) have received great attention for years due to their application in very-large-scale integration (VLSI) technology and their low resistivity and high thermal stability [1–3]. Among the metal silicides, titanium silicides exhibit the lowest resistivity and higher chemical stability than the others. Thus, they are used not only as an ohm contact material but also as a cold cathode material in field emission devices [4,5]. Actually, several different phases of Ti_3Si, Ti_5Si_4, Ti_5Si_3, TiSi, and $TiSi_2$ are formed under different conditions as shown in the Ti–Si phase diagram [6]. These titanium silicide phases show different structural and electrical properties. $TiSi_2$ [7] has a face-centered orthorhombic structure and a resistivity as low as 16–20 μΩ cm. It is mainly used as an interconnect. Ti_5Si_3 [8–10], however, has a hexagonal structure and shows a resistivity of 50–120 μΩ cm, which is slightly higher than that of $TiSi_2$. It is a promising material for high-temperature applications. Another compound, TiSi [4], has an orthorhombic structure and is found to have a resistivity of 60 μΩ cm, which is lower than that of Ti_5Si_3. With the development of device miniaturization, one-dimensional nanostructures have received much attention over the past decades because of their unique properties and potential applications [11–13]. Thus, titanium silicide nanostructures have attracted extensive interest due to their low resistivity, high thermal stability, large curvature at the top of the nanowires (NWs), and large surface area. $TiSi_2$ thin films covered by Ti_5Si_3 NWs are found to exhibit excellent field emission properties, despite Ti_5Si_3 showing a slightly higher resistivity [5].

The field emission properties of the TiSi NWs covering the $TiSi_2$ thin films are expected to be improved because the resistivity of the TiSi phase is lower than that of Ti_5Si_3. Therefore, it is important to investigate the formation of TiSi NWs on $TiSi_2$ thin films. Furthermore, the CVD method is one of the most widely used methods for preparing nanostructures with high purity [14]. Many freestanding titanium silicide NWs, such as $TiSi_2$ [15], TiSi [4,16], and Ti_5Si_3 NWs, have been successfully synthesized by the CVD method. The atmospheric pressure CVD (APCVD) method accepts full gaseous sources instead of consuming the Si or Ti substrate used normally in the CVD method and represents a cost-effective process for continuous large-scale production on many required substrates. Self-assembled NWs, such as TiSi NWs on Ti_5Si_3 thin films/glass substrates, have been successfully synthesized by the APCVD method [16–19]. In this paper, TiSi NWs synthesized on a $TiSi_2$ base layer on a glass substrate by the APCVD method are investigated in detail. The growth mechanisms for the formation of TiSi NWs on the $TiSi_2$ thin film are also considered.

2. Experimental details

Gaseous SiH_4 and liquid $TiCl_4$ were used as the Si and Ti precursors and gaseous N_2 was used as the dilution gas, respectively. Liquid $TiCl_4$ was heated to 38–41 °C via water bath until it vaporized enough, and then the vapor was carried by N_2 flow for the reaction. The SiH_4, $TiCl_4$ and N_2 were transported initially into a stainless steel chamber with a diameter of 5 cm and a length of 26.5 cm to mix for 40 s. Then they were introduced onto the glass substrates via a long quartz tube with a showerhead at its end for deposition. The samples were deposited in a vacuum chamber with a pressure of $7–9 \times 10^4$ Pa. The deposition process can be divided into two steps: first, a titanium silicide thin film was deposited, and second, titanium silicide NWs were formed, and the sample was kept in the vacuum chamber during the deposition. In

* Corresponding author. Tel.: +86 571 87952324; fax: +86 571 87952324.
E-mail address: dupy@zju.edu.cn (P. Du).

0925-8388/$ – see front matter © 2011 Elsevier B.V. All rights reserved.
doi:10.1016/j.jallcom.2011.04.108

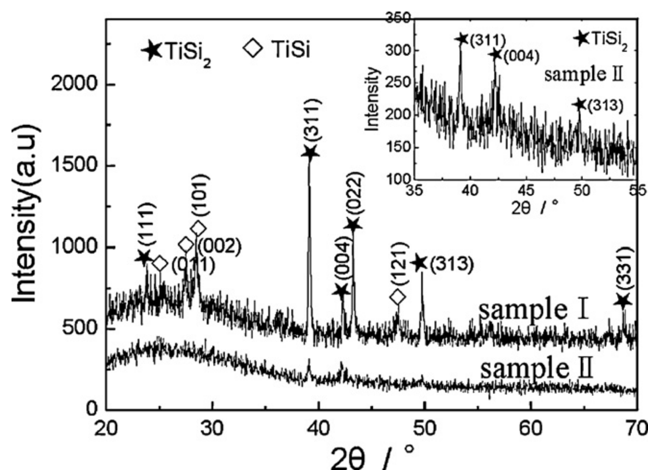

Fig. 1. XRD patterns of the titanium silicide thin films and nanowires (NWs) of sample I and sample II. The inset shows the XRD pattern of sample II with 2θ between 35° and 55°.

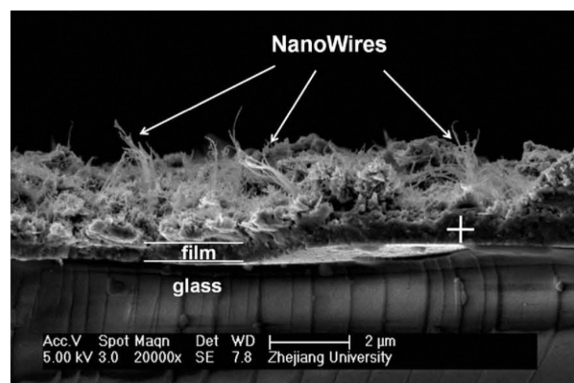

Fig. 2. Cross-sectional image of sample II. The white arrows indicate the NWs grown on the thin film. The white cross represents the point at which the EDX analysis is probed (see Fig. 3 below).

the first step, the gases were transported onto the glass substrate at a temperature of 720 °C for 3 min for sample I and 15 s for sample II, with a mole ratio of $SiH_4/TiCl_4$ of 4 for the deposition of the $TiSi_2$ thin films. The flow rates of SiH_4, $TiCl_4$, and N_2 were maintained at 21.2 sccm, 5.3 sccm, and 973.5 sccm, respectively, for sample I and 52.8 sccm, 13.2 sccm, and 734 sccm, respectively, for sample II. The flow rates of SiH_4 and N_2 were controlled by a rotameter and a mass control flowmeter, respectively, and the flow rate of $TiCl_4$ was controlled by the flow rate of the N_2 carrier gas. In the second step, the total gas flow rate and the deposition temperature were kept the same as those in the first step, while the ratio of SiH_4 to $TiCl_4$ was modulated to approximately 3. The flows of the reactive gases of SiH_4 and $TiCl_4$ were stopped while the N_2 was introduced into the gas mixing chamber to maintain the total gas flow rate of 1000 sccm for sample I and 800 sccm for sample II for additional reaction times of 15 min and 1 min, respectively. The concentrations of the reactive gases of SiH_4 and $TiCl_4$ were diluted naturally and exponentially during the second step. After the two deposition steps, the NWs covering on the thin films were deposited on the glass substrate.

Field emission-scanning electron microscopy (FE-SEM, SIRON, FEI) was used to observe the morphology of the samples. A Rigaku D/max diffractometer with Cu Kα radiation was used to characterize the structures of the NWs. The morphology of the NWs was observed by TEM. The microstructure of the NWs was evaluated using a JEOL-2010 high-resolution transmission electron microscopy (HRTEM). The chemical composition of the samples was analyzed using energy dispersive X-ray spectroscopy (EDX). The samples of the NWs for observation by TEM and HRTEM were prepared as follows: first, the samples were immersed in an ethanol solution and dispersed by an ultrasonic oscillator for 15 min; second, the dispersed solutions containing the NWs were dropped on a carbon-covered copper grid; and third, the copper grids were used for observation after drying.

3. Results and discussion

Fig. 1 shows the XRD patterns of sample I and sample II deposited at a flow rate ratio of $SiH_4/TiCl_4$ of 4. The inset in Fig. 1 shows the XRD pattern of sample II with 2θ between 35° and 55°. A $TiSi_2$ crystalline phase with face-centered orthorhombic structures was formed in these two samples, as shown in Fig. 1. In addition, a small amount of TiSi crystalline phase obviously formed in sample I, as shown in Fig. 1. The quantity of the $TiSi_2$ crystalline phase in sample I is higher than that of sample II, as exhibited in Fig. 1. Fig. 2 shows the cross-sectional image of sample II as-deposited. The three layers of the glass substrate, the thin film and the NWs are present from bottom to top, and the thickness of the thin film is approximately 500 nm. This implies that the thin films form on the glass substrates in the first stage, and then the NWs grow on the thin films during the second stage. Fig. 3 shows the EDX spectrum of the thin film. The probe position is marked as a "+" in Fig. 2. The results of the EDX reveal that the atomic ratio of Si to Ti in the thin film is 2.3:1, which shows the formation of the $TiSi_2$ phase in the thin films in addition to the TiSi phase as the Si content in the $TiSi_2$ phase is higher than that of the TiSi phase. The TEM morphology of a single nanowire of the samples is exhibited in Fig. 4. As shown in Fig. 4a, there are no spherical particles at the tip of the nanowire, which is normally reported for NWs grown by the VLS mechanism [20]. It can be deduced that no catalysts were used during the formation processes. The high-resolution TEM image of the nanowire is shown in Fig. 4b. The inset in Fig. 4b shows the selected area electron diffraction (SAED) pattern of the NWs, showing reciprocal lattice peaks along the different lattice directions, which is indexed to be orthorhombic single-crystal TiSi phase. The growth front of the NWs is along the direction that is perpendicular to its (1 1 0) plane, as shown in Fig. 4a and b. The TEM morphology of a single nanowire of sample II is exhibited in Fig. 4c. No particle is observed at the top of the nanowire. Fig. 4d shows the high-resolution TEM image of the nanowire of sample II. The inset in Fig. 4d shows the selected area electron diffraction (SAED) pattern of the nanowire. It exhibits the formation of the orthorhombic TiSi single-crystal NWs. The growth front of the NWs is along the specific direction that is perpendicular to their (1 1 0) planes, as exhibited in Fig. 4c and d. As a result, the $TiSi_2$ thin films were formed on the glass substrates, and then the TiSi single-crystal NWs were successfully formed on the $TiSi_2$ thin films as-prepared.

Fig. 5a–c shows the SEM images of sample I at different magnifications while Fig. 5d shows the morphology of sample II. A large area of NWs was formed on the thin films, as shown in Fig. 5a. The NWs had a length of 1–2 µm, as shown in Fig. 5b and c for sample I and in Figs. 2 and 5d for sample II. The thickness of the NWs was between 15 and 50 nm, as shown in Fig. 5c for sample I and Fig. 5d for sample II. Both the thickness and the length of the NWs for sample I and sample II have no obvious differences, although the deposition conditions were varied.

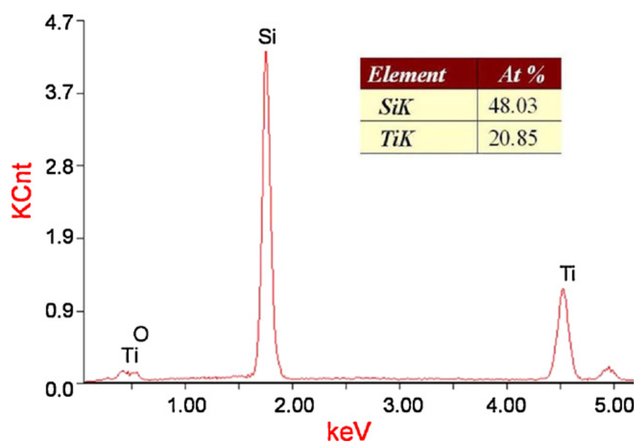

Fig. 3. EDX analysis at a point marked by a "+" as shown in Fig. 2.

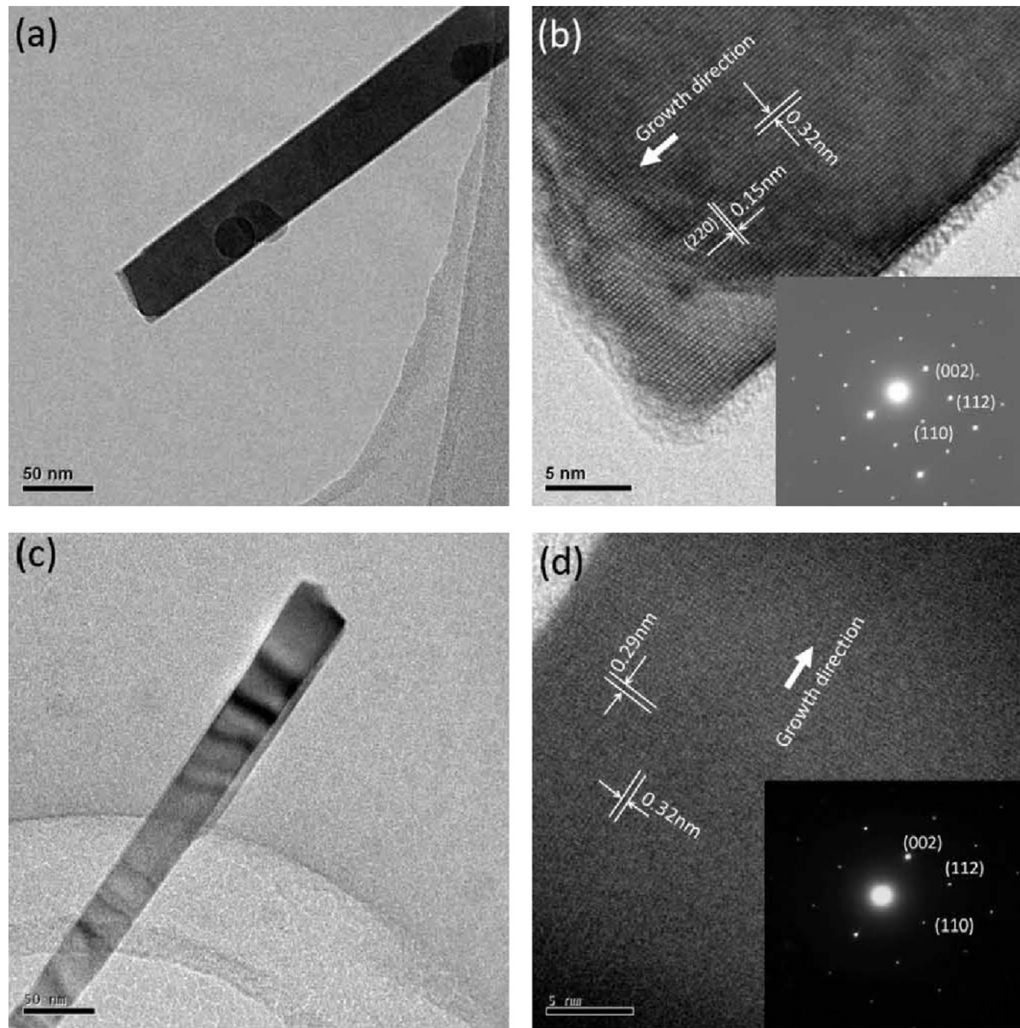

Fig. 4. The TEM images of a single TiSi nanowire of (a), (b) sample I and (c), (d) sample II. The insets in Fig. 4(b) and (d) show the selected area electron diffraction (SAED) patterns of sample I and sample II, respectively.

During the first step, source gases with a flow rate ratio of $SiH_4/TiCl_4$ of 4 were used for deposition. The reactions probably occurred thermodynamically as shown below.

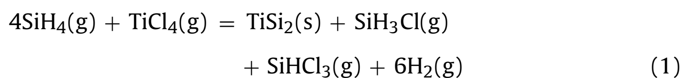

$$4SiH_4(g) + TiCl_4(g) = TiSi_2(s) + SiH_3Cl(g) + SiHCl_3(g) + 6H_2(g) \quad (1)$$

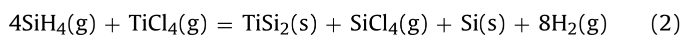

$$4SiH_4(g) + TiCl_4(g) = TiSi_2(s) + SiCl_4(g) + Si(s) + 8H_2(g) \quad (2)$$

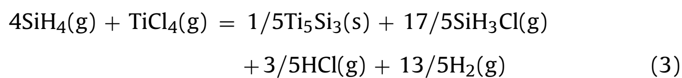

$$4SiH_4(g) + TiCl_4(g) = 1/5Ti_5Si_3(s) + 17/5SiH_3Cl(g) + 3/5HCl(g) + 13/5H_2(g) \quad (3)$$

The Gibbs free energies [21] of reactions (1)–(3) are −449.079 KJ, −504.419 KJ, −414.973 KJ at 1000 K, respectively. Although all of the reactions shown above are likely to occur, the reaction shown in Eq. (2) is most likely to happen thermodynamically compared to those of the other equations due to its negative free energy with the largest absolute value of −504.419 KJ at 1000 K. Furthermore, no Ti_5Si_3 crystalline phase was found other than the $TiSi_2$ phase as shown in Fig. 1. This indicates that the reaction below probably occurs following reaction (3)

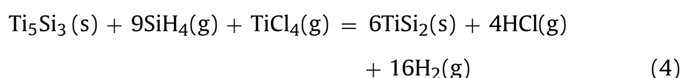

$$Ti_5Si_3(s) + 9SiH_4(g) + TiCl_4(g) = 6TiSi_2(s) + 4HCl(g) + 16H_2(g) \quad (4)$$

The Gibbs free energy of that reaction is −1037.412 KJ at 1000 K, which is also very low. The Ti_5Si_3 formed from reaction (3) most likely serves as one of the reactants in reaction (4) to form ultimately $TiSi_2$. Therefore, the $TiSi_2$ thin films are finally formed on the glass substrates in this case.

Moreover, as exhibited in Fig. 1, the quantity of the $TiSi_2$ crystalline phases in sample I is higher than that of sample II. This can be attributed, in fact, to a thickness limitation with regard to measuring the crystallinity in the thin film. Actually, there is a limitation on the detection of thickness when using XRD technology to measure thin films. If the thin film dimension is larger than the limitation, then the sample thickness is not an indicator of crystallinity. However, the thicknesses of the thin films that were prepared are on the order of several micrometers, which did not reach the thickness limitation for XRD measurements in this work. The peak intensity in the XRD pattern will thus increase with the increase in the thickness of the thin films rather than with the crystallinity. In fact, the thickness of the thin films formed in sample I is approximately 2 μm, which is about 4 times thicker than that of sample II. The larger quantity of the crystalline phase in sample I is attributed apparently to the greater thickness of the thin film with a long deposition time, although the concentration of the source gases in sample I is lower than that of sample II. Because the quantity of the crystalline phase is mainly generated by the increase in thickness, the $TiSi_2$ thin films deposited at the first stage under different conditions

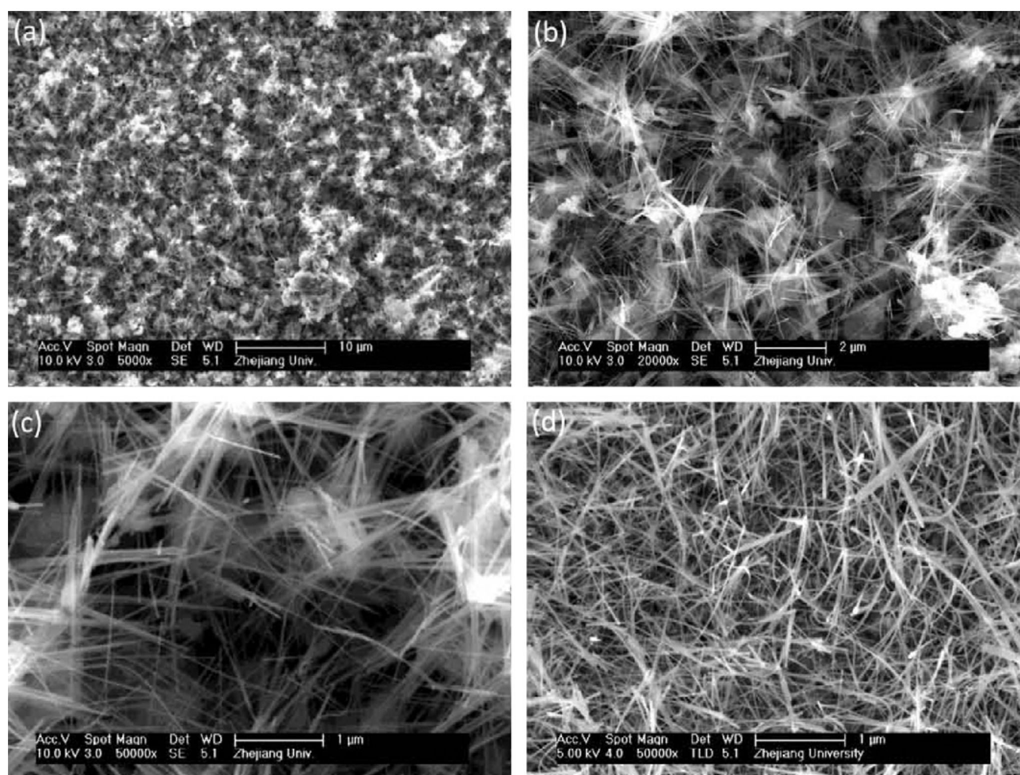

Fig. 5. SEM images of (a)–(c) sample I with different magnifications and (d) sample II, respectively.

likely show the same quantity of the $TiSi_2$ crystalline phase in their surfaces. Therefore, the $TiSi_2$ crystalline phase-contained thin films deposited in the first step are used as a layer supplying nucleation site, inducing the formation of stable NWs on the thin layers in a way almost independent of the deposition conditions used in this work.

After forming the crystalline layer of $TiSi_2$, source gases with a flow rate ratio of $SiH_4/TiCl_4$ of 3 were used, and the concentrations of the reactive gases of SiH_4 and $TiCl_4$ in the total gas were diluted naturally and exponentially. As a second step, the reaction is likely:

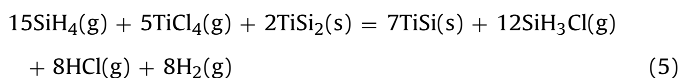

$$15SiH_4(g) + 5TiCl_4(g) + 2TiSi_2(s) = 7TiSi(s) + 12SiH_3Cl(g) + 8HCl(g) + 8H_2(g) \quad (5)$$

where the Gibbs free energy of the reaction at 1000 K is −1455.899 KJ [21]. This means that the reaction is thermodynamically favorable.

In traditional VLS mechanisms for NW preparation, metal catalysts often tend to form a liquid alloy droplet with a relatively low solidification temperature. A metal-containing liquid nanoparticle normally forms at the growth frontier of the NWs, acting as a catalytic active site. However, there are no particles being observed at the ends of the NWs in this work, as shown above. In the system of Ti and Si, the lowest liquid eutectic point of Ti and Si shown on the equilibrium phase diagram is 1330 °C, which is markedly above 720 °C, the temperature at which the titanium silicide NWs form in this work. It seems that the liquid alloy droplet cannot be formed if there are no catalysts used in this case. Therefore, the growth of the TiSi NWs cannot be explained by the traditional VLS mechanisms, which are widely used to illustrate the growth of NWs.

Actually, as shown in Fig. 6, when the source gases of SiH_4 and $TiCl_4$ are introduced onto the nucleating layer of $TiSi_2$ during the second step, the TiSi nuclei are most likely formed on the $TiSi_2$ layer, according to reaction (5). The TiSi nuclei serve unambiguously as seeds for further growth of the TiSi crystalline phase. TiSi nano-islands are thus formed widely on the $TiSi_2$ nucleating layer. The TiSi nano-islands are very active as the dimension of the TiSi islands is on the nano-scale, and thus, they present a quasi-liquid state character and dissolve atoms, as demonstrated in our previous papers [16,17]. The Ti and Si atoms can be dissolved into the quasi-liquid nano-islands easily with continuous feeding of the source gases of SiH_4 and $TiCl_4$. Finally, the TiSi phases grow continuously by supersaturating the Ti and Si atoms in the separating TiSi nano-islands, except for some that grow with the depositing of a few atoms on the surface of the TiSi phases.

In fact, it is very difficult for the nuclei to grow up and form a continuous thin film in this case due to the anisotropic growth of the crystalline phase. The lower the surface energy is, the easier the surface will stretch out as an outer plane. As a result, the TiSi phase would be formed with the lowest surface energy. When the TiSi crystalline phase begins to form on the nano-islands, a competition in the growth rate among different crystallographic planes begins. The larger the number of atoms per unit area of the plane is, the lower the surface energy of the crystallographic plane will be. As seen in Fig. 7, it has been calculated that the numbers of atoms per unit area of the (0 0 2) and (1 1 0) planes of the TiSi crystalline phase are the largest and the second largest, respectively. Therefore, the surface-free energies of the (0 0 2) and (1 1 0) planes are the lowest and the second lowest, correspondingly. As the TiSi nucleus forms, any of the crystallographic planes will be exposed as an outer surface plane of the crystalline phase. However, a plane that has the lowest surface energy is the easiest to form and the easiest to grow as an outer surface. As the TiSi crystalline phase forms, the (0 0 2) and the (1 1 0) planes are expected to grow as outer surfaces more easily compared to other planes. However, the surface-free energy of the (0 0 2) plane is lower than that of the (1 1 0) plane. The increase in surface area of the (0 0 2) plane rather than of the (1 1 0) plane will lower the surface energy per unit area of the TiSi crystalline phase. Therefore, the surface area of the (0 0 2) plane increases spontaneously and rapidly, while the surface area of

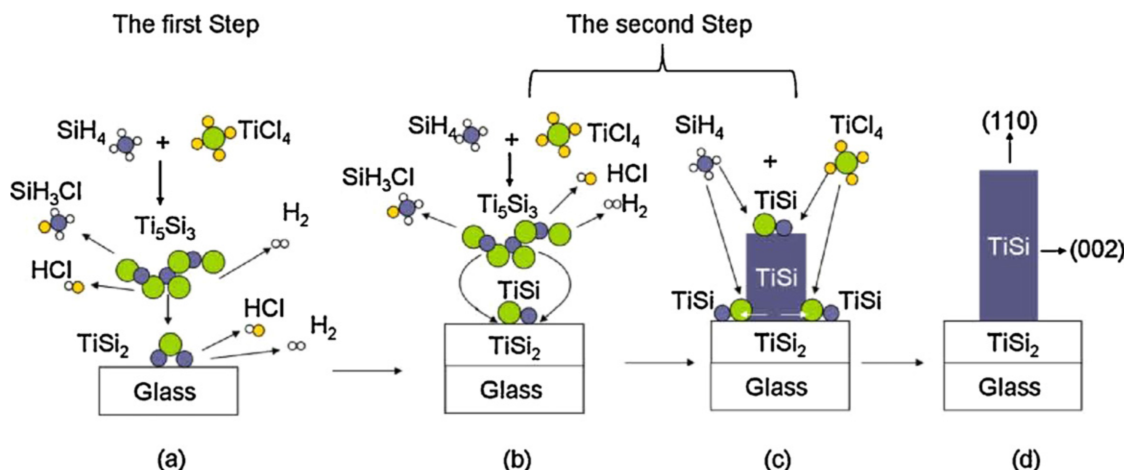

Fig. 6. Proposed growth process for the formation of the titanium silicide thin films and NWs. (a) Deposition of the preliminary layer of $TiSi_2$ thin films on the glass substrate, (b) Formation of the TiSi nano-islands on the $TiSi_2$ thin films, (c) "self-catalysis" growth of the TiSi NWs and (d) the final TiSi NWs formed on the $TiSi_2$ thin films.

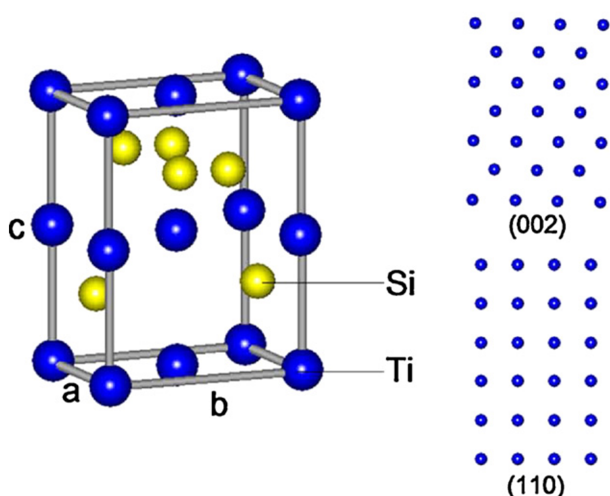

Fig. 7. Schematic representation of the TiSi structured cell.

the (1 1 0) plane, being perpendicular to the (0 0 2) plane, increases only slightly. Consequently, served by the quasi-liquid Ti–Si nano-islands as seeds, the TiSi NWs form and grow along the direction perpendicular to the (1 1 0) planes of the TiSi crystalline phases with an increase in the surface area of the (0 0 2) planes, as exhibited in Fig. 4b and d. Simultaneously, Ti and Si atoms will deposit on the outer surface of the NWs directly and contribute to the continuous growth of the NWs. The formation process of the TiSi NWs by the two-step method is graphically represented in Fig. 6. The formation of the TiSi NWs without using any catalysts is called "self-catalysis" growth, which is similar to that of the "VS" mechanism [22].

Finally, a large quantity of TiSi NWs is formed by the two-step method, as shown in Fig. 5. The NWs are formed in the second step, in which the nucleation of the NWs in the thin film relates to the modulation of both the total concentrations of the source gases and the deposition times within a certain range in the first step. Neither the thicknesses nor the lengths of the NWs for sample I and sample II show any difference between the two samples, despite the deposition conditions being varied. This shows that the morphology of the NWs formed in this case is almost stable.

4. Conclusions

A large quantity of TiSi NWs with orthorhombic structures have been successfully prepared on the synchronously deposited nucleating layer of the face-centered orthorhombic $TiSi_2$ crystalline layer by a two-step APCVD method without using any catalysts. The formation of the TiSi NWs originates from the TiSi nano-islands that are induced by the nucleating layer of the synchronously deposited $TiSi_2$ crystalline phase under favorable thermodynamic conditions. As the source gases dissolve in the Ti–Si nano-islands, the TiSi crystalline phases precipitate and grow continuously with both the supersaturation of Ti and Si atoms in the nano-islands and the deposition of Ti and Si atoms directly on the surfaces of the TiSi crystalline phases that form. The anisotropic growth of the TiSi crystalline phases occurs due to the different surface-free energy, which result in the formation of the NWs and the growth of the NWs along the directions perpendicular to the (1 1 0) planes. The "self-catalysis" mechanism dominates the growth of the TiSi NWs in the case of the APCVD processes. The TiSi NWs combined with the $TiSi_2$ thin films are expected to be used as assembled nano-electrodes in future multifunctional nano-devices.

Acknowledgments

This work is supported by NSFC (Grant No. 50672084), the National Key Scientific and Technological Project (Grant No.2009CB623302) and Fundamental Research Funds for the Central Universities, China.

References

[1] C. Wen, A. Kato, T. Nonomura, H. Tatsuoka, J. Alloys Compd. 509 (2011) 4583–4587.
[2] D. Connétable, O. Thomas, J. Alloys Compd. 509 (2011) 2639–2644.
[3] W.J. Yao, N. Wang, J. Alloys Compd. 487 (2009) 354–357.
[4] H.-K. Lin, H.-A. Cheng, C.-Y. Lee, H.-T. Chiu, Chem. Mater. 21 (2009) 5388–5396.
[5] H.-K. Lin, Y.-F. Tzeng, C.-H. Wang, N.-H. Tai, I.-N. Lin, C.-Y. Lee, H.-T. Chiu, Chem. Mater. 20 (2008) 2429–2431.
[6] C.L. Yeh, H.J. Wang, W.H. Chen, J. Alloys Compd. 450 (2008) 200–207.
[7] J. Du, P. Du, M. Xu, P. Hao, Y. Huang, G. Han, C. Song, W. Weng, J. Wang, G. Shen, J. Appl. Phys. 101 (2007) 033539.
[8] D. Vojtech, P. Novak, P. Machac, M. Mort'anikova, K. Jurek, J. Alloys Compd. 464 (2008) 179–184.
[9] Y. Zhana, X. Zhang, J. Hu, Q. Guo, Y. Du, J. Alloys Compd. 479 (2009) 246–251.
[10] P. Novák, F. Průša, J. Šerák, D. Vojtěch, A. Michalcová, J. Alloys Compd. 504 (2010) 320–324.
[11] C. Gu, J. Huang, Y. Wu, M. Zhai, Y. Sun, J. Liu, J. Alloys Compd. 509 (2011) 4499–4504.
[12] S. Zanganeha, M. Torabi, A. Kajbafvala, M.R. Navid Zanganeh, Bayati, H.R. Roya Molaei, S.K. Zargar, Sadrnezhaad, J. Alloys Compd. 507 (2010) 494–497.
[13] G. Meng, X. Fang, Y. Zhou, J. Seo, W. Dong, S. Hasegawa, H. Asahi, H. Tambo, M. Kong, L. Li, J. Alloys Compd. 491 (2010) 72–76.
[14] D.-S. Kanga, H.S. Lee, S.K. Han, V. Srivastava, E.S. Babu, S.-K. Hong, M.-J. Kim, J.-H. Song, J.-H. Song, H. Kim, D. Kim, J. Alloys Compd. 509 (2011) 5137–5141.

[15] S. Zhou, X. Liu, Y. Lin, D. Wang, Chem. Mater. 21 (2009) 1023–1027.
[16] J. Du, P. Du, P. Hao, Y. Huang, Z. Ren, W. Weng, G. Han, G. Zhao, Nanotechnology 18 (2007) 345605.
[17] J. Du, P. Du, P. Hao, Y. Huang, Z. Ren, G. Han, W. Weng, G. Zhao, J. Phys. Chem. C 111 (2007) 10814.
[18] J. Du, Z. Ren, K. Tao, A. Hu, HaoF P., Y. Huang, G. Zhao, W. Weng, G. Han, P. Du, Cryst. Growth Des. 8 (2008) 3543–3548.
[19] Z. Ren, A. Hu, K. Tao, J. Du, W. Weng, N. Ma, P. Du, Thin Solid Films 517 (2009) 5014–5017.
[20] S.R. Hejazi, H.R. Madaah Hosseini, M. Sasani Ghamsari, J. Alloys Compd. 455 (2008) 353–357.
[21] G.J. Reynolds, C.B. Cooper III, P.J. Gaczi, J. Appl. Phys. 65 (1989) 3212–3218.
[22] S.L. Wang, X. Jia, P. Jiang, H. Fang, W.H. Tang, J. Alloys Compd. 502 (2010) 118–122.